Protonation of the oxo-bridged heme/copper assemblies: Modeling the oxidized state of the cytochrome *c* oxidase active site

By: Maria C. Carrasco, Katherine J. Dezarn, Firoz Shah Tuglak Khan, Shabnam Hematian

Maria C Carrasco, Katherine J Dezarn, Firoz Shah Tuglak Khan, Shabnam Hematian. 2021. Protonation of the oxo-bridged heme/copper assemblies: Modeling the oxidized state of the cytochrome c oxidase active site. *Journal of Inorganic Biochemistry 225*, 111593. https://doi.org/10.1016/j.jinorgbio.2021.111593

Abstract:

In this study on model compounds for the resting oxidized state of the iron-copper binuclear center in cytochrome *c* oxidase (C*c*O), we describe the synthesis of a new μ-oxo-heme/Cu complex, [(TPP)Fe^{III}–O–Cu^{II}(tmpa)][$B(C_6F_5)_4$] (**2**) {TPP: tetraphenyl porphyrinate(2–); TMPA: *tris*(2-pyridylmethylamine)}, as well as two protonation events for three μ-oxo-heme/Cu complexes with varying peripheral substituents on the heme site. The addition of increasing amounts of strong acid to these μ-oxo-heme/Cu systems successively led to the generation of the corresponding μ-hydroxo, μ-aquo, and the dissociated complexes. The heme/Cu assemblies bridged through a water ligand are reported here for the first time and the ^{1}H NMR and ^{19}F NMR spectral properties are consistent with antiferromagnetically coupled high-spin iron(III) and copper(II) centers. By titration using a series of protonated amines, the pK_a values for the corresponding μ-hydroxo-heme/Cu species (i.e., the first protonation event) have been reported and compared with the pK_a ranges previously estimated for related systems. These synthetic systems may represent structural models for the oxidized Fe^{III}–X–Cu^{II} resting state, or turnover intermediates and can be employed to clarify the nature of proton/electron transfer events in C*c*O.

Synopsis: The resting oxidized state of the cytochrome *c* oxidase active site contains an Fe_{a3}–OH_x–Cu_B moiety. Here, we investigated two successive protonation events, for a series of μ-oxo-heme/Cu assemblies and reported the pK_a values for the first protonation event. The μ-aquo-heme/Cu complexes described here are the first examples of such systems.

Graphical abstract:

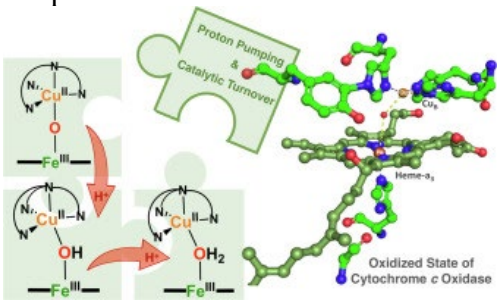

Keywords: cytochrome *c* oxidase | bridging ligand | protonation | acid dissociation constant | paramagnetic NMR | antiferromagnetic coupling

Article:

At the heart of mitochondrial respiratory processes, cytochrome *c* oxidase (C*c*O) enables the four-electron reduction of dioxygen (O_2) to water at its heme-a_3/Cu_B binuclear center [1]. In the active (**O_H**) or as-isolated (**O**) oxidized state of the enzyme, the Fe_{a3} and Cu_B sites are within ~4–5 Å from one another and exhibit a strong antiferromagnetic coupling through a bridging-ligand revealed by electron pragmatic resonance (EPR) and magnetic susceptibility studies [2,3]. Later, the extended X-ray absorption fine structure (EXAFS) and resonance Raman spectroscopic results along with a combination of theoretical and advanced crystallographic studies indicated that Cu_B shares an oxygen-based ligand with heme-a_3, the protonation state of which is still under debate (i.e., water, hydroxo, or oxo; Fig. 1) [[4], [5], [6], [7], [8], [9]]. The subtle change in the protonation state of this bridging-ligand could significantly alter the electron and proton transfer events at the bimetallic center and the overall proton translocation across the mitochondrial inner membrane.

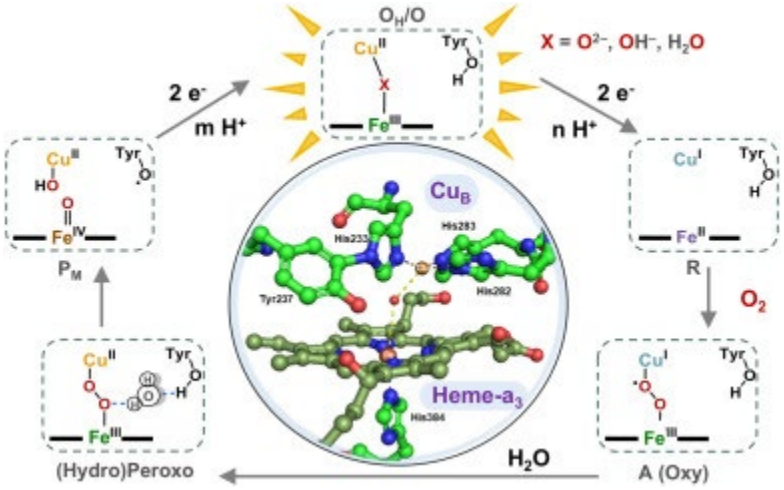

Fig. 1. C*c*O reduces dioxygen via the proposed intermediates shown. The oxidized state of the enzyme with the O-based bridging-ligand is highlighted on the top. The highly conserved covalent His-Tyr cross-link shown in the active site is also essential for the oxidase function of C*c*O [1].

Initial attempts by Karlin and co-workers to model the heme-a_3/Cu_B and dioxygen chemistry led to the discovery of μ-oxo-heme/Cu complexes, $[(P)Fe^{III}–O–Cu^{II}(L)]^+$, in which the bridging-oxo is derived from O_2, is very basic and, in most cases, can be reversibly protonated to give the μ-hydroxo species, $[(P)Fe^{III}–OH–Cu^{II}(L)]^{2+}$ [[10], [11], [12]]. The protonation results in significant structural changes including bending of the Fe–O(H)–Cu moiety, lengthening of both metal-O(H) bonds, and lowering the degree to which the iron atom is pulled out of the porphyrin plane.

F_8TPP, *tetrakis*(2,6-difluorophenyl) porphyrinate(2−); TPP, tetraphenyl porphyrinate(2–); TMPP, *tetrakis*(4-methoxyphenyl) porphyrinate(2−); TMPA, *tris*(2-pyridylmethylamine)

To date, the pK_a ranges have been estimated for only three of these μ-hydroxo-heme/Cu systems [13] as shown in Fig. 2 [[14], [15], [16], [17]].

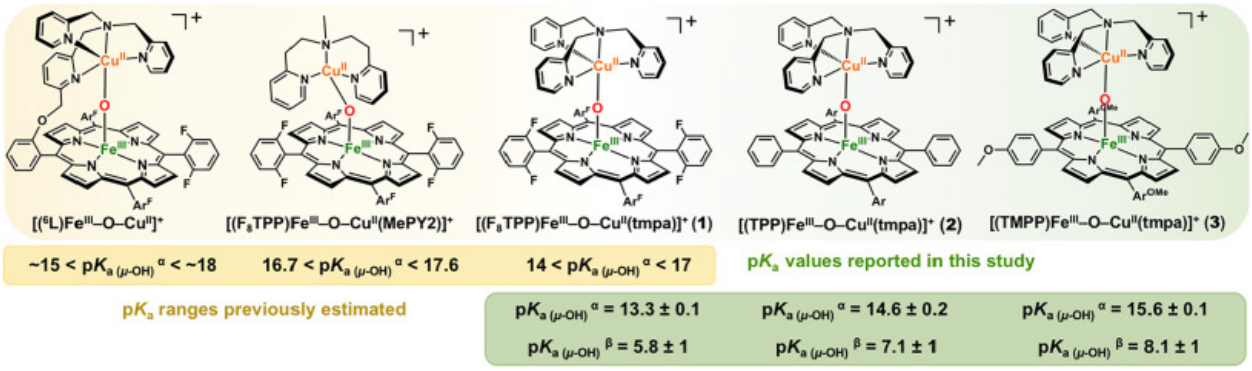

Fig. 2. Structures of the synthetic μ-oxo-heme/Cu complexes investigated for the basicity of their bridging-oxo moiety. The pK$_a$ ranges and values given are in MeCN$^{\alpha}$ or converted by subtracting 7.5 ± 1 units for the estimated values in water$^{\beta}$. MePY2: *N,N*-bis[2-(2-pyridyl)ethyl]methylamine.

In this report, we have used a range of protonated nitrogen bases (i.e., weak acids) that are paired with the bulky and non-coordinating counterion *tetrakis*(pentafluorophenyl)borate, $[B(C_6F_5)_4]^-$, with known pK_a values spanning from 12.30 to 18.46 in MeCN (Table S1) for measuring acid dissociation constants for a series of μ-hydroxo-heme/Cu systems. Here, we investigate three μ-oxo-heme/Cu assemblies, all bearing a tripodal tetradentate pyridyl-alkylamine copper chelate, *tris*-2-pyridylmethylamine (TMPA), and porphyrinate rings with varying peripheral substituents; i.e., $[(F_8TPP)Fe^{III}–(OH)–Cu^{II}(tmpa)]^{2+}$ (**1-H**$^+$), the novel complex, $[(TPP)Fe^{III}–(OH)–Cu^{II}(tmpa)]^{2+}$ (**2-H**$^+$), and $[(TMPP)Fe^{III}–(OH)–Cu^{II}(tmpa)]^{2+}$ (**3-H**$^+$) (Fig. 2), {F_8TPP: *tetrakis*(2,6-difluorophenyl) porphyrinate(2−); TPP: tetraphenyl porphyrinate(2–); TMPP: *tetrakis*(4-methoxyphenyl) porphyrinate(2−)}. We also discuss the second protonation event that generates μ-aquo-heme/Cu assemblies which are the first examples of such complexes bridged through a water ligand.

Titration experiments using acids with the appropriate pK_a range were first monitored using UV–vis spectroscopy. The Soret bands of the starting μ-oxo complexes are considerably red-shifted (i.e., λ_{max} = 437, 441, and 445 nm for **1**–**3** in dichloromethane (DCM), respectively) relative to those of classical high-spin ferric hemes [12]. First protonation of the bridging-oxo moiety with weak acids results in a significant blue-shift of Soret bands (e.g., **3-H**$^+$; λ_{max} = 418 nm, Fig. 3a) and complete and clean conversion to the corresponding μ-hydroxo species. The addition of a strong base also gave back the starting μ-oxo complex (Fig. S21).

Additionally, the final spectra were identical in all regards to those of the authentic μ-hydroxo samples generated from the addition of one equivalent of a very strong acid such as protonated diethyl ether, i.e., $[H(OEt_2)_2][B(C_6F_5)_4]$, to the corresponding μ-oxo complexes (Fig. 3b).

As expected, on passing from the electron-deficient F_8TPP ring to the electron-rich TMPP ligand, [18] with enhanced electron density around the iron center, pK_a increased (Fig. 2) [19].

Interestingly, adding excess amounts of strong acid to the authentic μ-hydroxo sample led to further blue-shifts of the Soret bands and consequently formed two new species. Perhaps initially a bridged-aquo species formed, $[(P)Fe^{III}–(H_2O)–Cu^{II}(L)]^{3+}$, which later underwent dissociation generating the monomer complexes, i.e., $[(P)Fe^{III}(Et_2O)_2]^{+}$ and $[(tmpa)Cu^{II}(Et_2O)]^{2+}$. The presence of the two bridged species is more prominent in the Q-band region of the UV–vis spectra (Fig. 3b).

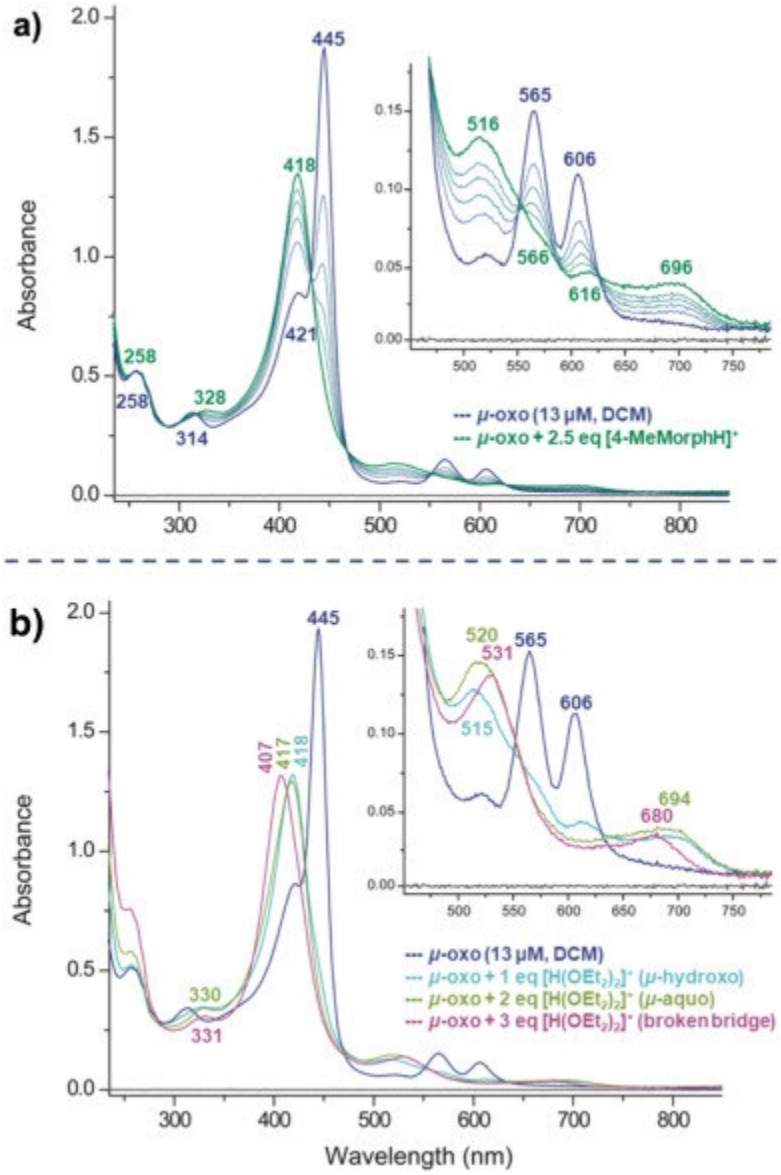

Fig. 3. Titration of **3** with a weak or strong acid in DCM as monitored by UV–vis spectroscopy: Full formation of the **3-H**$^{+}$ after addition of (a) 2.5 equiv. of [4-MeMorphH][$B(C_6F_5)_4$] or (b) 1 equiv. of [$H(OEt_2)_2$][$B(C_6F_5)_4$]. The addition of the second and third equiv. of the strong acid leads to the formation of the μ-aquo complex and the breaking of the bridging ligand bonds, respectively. The final spectrum is identical to the spectrum of authentic $[(TMPP)Fe^{III}(THF)_2]^{+}$ compound.

To better understand these protonation events and whether the copper and iron centers remain connected through a bridging-ligand in both μ-hydroxo and suspected μ-aquo complexes, nuclear magnetic resonance (NMR) spectroscopy was used. The ^{1}H NMR spectra of the complexes **1**–**3** are consistent with antiferromagnetically coupled high-spin ferric and cupric centers (S = 2) and displayed distinct resonates for the heme center at around 65.5 ppm for the pyrrolic protons and in the 7–10 ppm range for the *meso*-aryl protons while the upfield-shifted signals (−89.2, −22.6, −6.25, 4.45 ppm in **2**) were assigned to protons of the TMPA moiety [20]. The latter signature upfield peaks are due to the dipolar interactions of the TMPA protons with half-filled $d_{xz,yz}$ orbitals of the ferric heme moiety as well as aromatic ring current effects of the porphyrin ligand (Fig. 4).

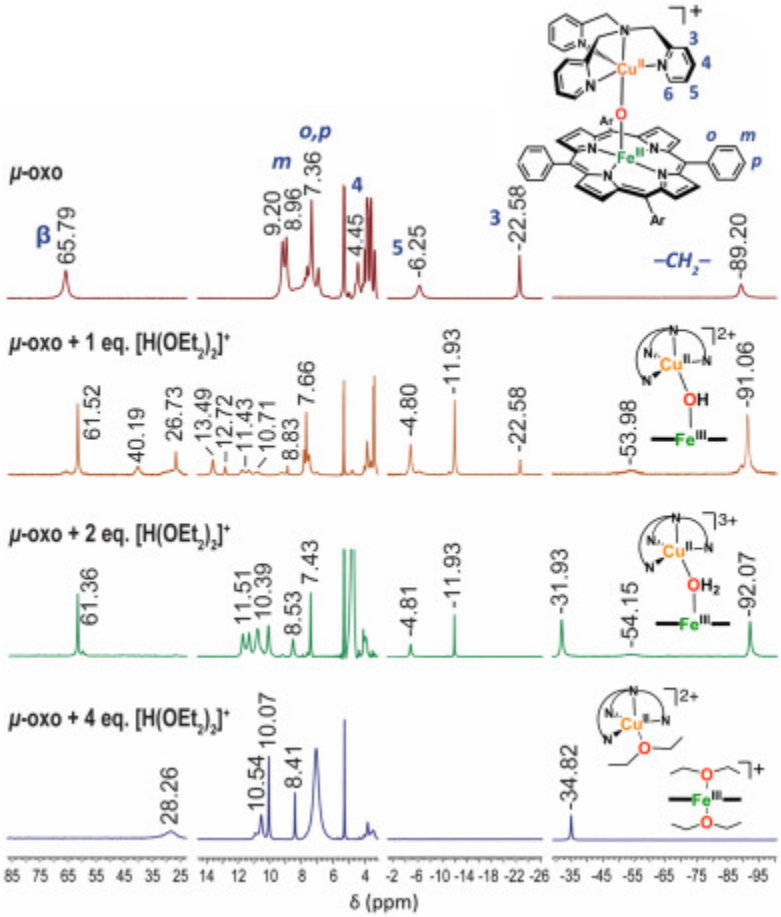

Fig. 4. Titration of **2** with the strong acid as monitored by ^{1}H NMR spectroscopy: Spectra of 2 in DCM-d_2 followed by addition of increasing quantities of $[H(OEt_2)_2][B(C_6F_5)_4]$. The addition of more than 2 equiv. of the strong acid was accompanied by release of the bridging ligand and breaking of the magnetic coupling between the copper and iron centers.

The addition of the second equivalent of $[H(OEt_2)_2][B(C_6F_5)_4]$, displayed changes consistent with the formation of μ-hydroxo-heme/Cu species (Fig. 4). As expected, the protonation of the bridging-oxo moiety was slow in the NMR timescale [21]; hence distinct sets of peaks were observed for individual species. Signals for the TMPA moiety of **2-H**$^{+}$ were still observed in the upfield region of the spectrum (−91 to 4.5 ppm), confirming strong coupling between the metal

centers, and the signal for the β–pyrrole protons, remained downfield shifted (~61.5 ppm). Strikingly, the 6-pyridyl proton resonance in the μ-hydroxo complex became observable at ~– 54 ppm, possibly due to increased distance to the heme site and decreased broadening of the signal [22].

Upon adding the third equivalent of the strong acid, a shift in the spectrum to a new complex was observed, similar to that noted in the UV–vis experiment. A distinguished upfield shift was observed at about −92 ppm suggesting the new complex remains intact, or that the copper moiety stayed bound to the heme through a likely water ligand (Fig. 4 and Fig. S24). This μ-aquo-heme/Cu assembly is in agreement with the recent proposed structure for the **O** state of C*c*O reported by Noodleman and co-workers [7]. Further addition of the strong acid led to protonation of the bridging water ligand [23] and dissociation of the heme/Cu assembly [24].

The molecular structure of the heme, $[(F_8TPP)Fe^{III}(Et_2O)_2]^+$, was also obtained from the reaction

mixture of **1** and strong acid by single crystal X-ray crystallography (Fig. 5). The Fe O bond distances are similar to those reported for $[(F_8TPP)Fe^{III}(THF)_2]^+$ [25].

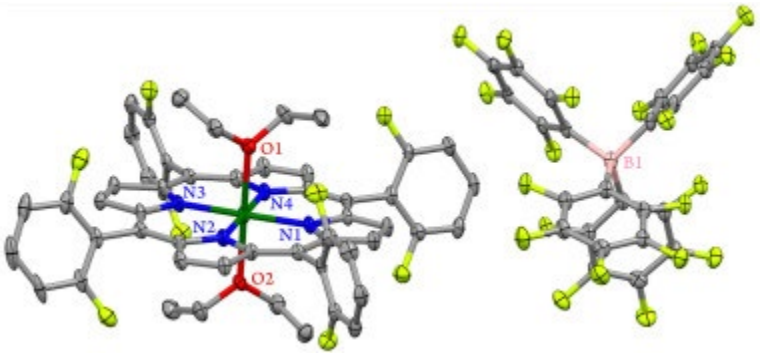

Fig. 5. Displacement ellipsoid plot (50% probability level) of $[(F_8TPP)Fe^{III}(Et_2O)_2][B(C_6F_5)_4]$, showing the atom-labeling scheme. Hydrogen atoms have been omitted for clarity. Selected bond lengths (Å) and angles (deg): Fe1–O1, 2.203(4); Fe1–O2, 2.171(3); Fe1–N1, 2.023(4); Fe1–N2, 2.015(3); Fe1–N3, 2.020(4); Fe1–N4, 2.011(3); O2–Fe1–O1, 178.51(13); N1–Fe1–N2, 91.01(14); N1–Fe1–N3, 179.38(17); N1–Fe1–N4, 89.24(14); N1–Fe1–O1, 88.80(14); N1–Fe1–O2, 90.41(15); N2–Fe1–N3, 88.89(14); N2–Fe1–N4, 179.41(17); N2–Fe1–O1, 88.26(14); N2–Fe1–O2, 90.49(14); N3–Fe1–N4, 90.86(14); N3–Fe1–O1, 90.59(15); N3–Fe1–O2, 90.20(14); N4–Fe1–O1, 92.28(15); N4–Fe1–O2, 88.98(14).

Titration of **1** was also monitored through ^{19}F NMR spectroscopy and the change in the splitting pattern for the fluorines on five-coordinated axially symmetric heme provided additional support for our proposition that during the first and second protonation events the heme/Cu assemblies remain connected through the hydroxo- and aquo-ligand. Here, each protonation event and subsequent bending of the bridge alters the molecular symmetry (Fig. S23).

The data from both UV–vis and NMR measurements indicate that the first protonation of the oxo moiety forms a μ-hydroxo complex followed by the conversion to an aquo-bridged species, upon the next protonation event. The pK_a values in MeCN are about 7.5 ± 1 units greater than in water [26,27]. Thus, the pK_a values reported here (Fig. 2) are consistent with the value of 8.8 obtained

through pH titration for a recent water soluble supramolecular heme/Cu system [28]. These values are particularly important as the pK_a value of the tyrosine residue covalently cross-linked to one of the histidine ligands of Cu_B in C*c*O have been estimated to be ~8.5 [[29], [30], [31], [32]]. This is in agreement with the previously proposed role of the cross-linked tyrosine as a potential proton donor/acceptor in the oxidized state(s) of the enzyme [1,33]. Therefore, understanding the protonation states and pK_a values of the bridging-ligands in $\mathbf{O}_H$ and **O** will help illustrate their relationships to the proton-pumping function and/or turnover of C*c*O.

Acknowledgments

The authors gratefully acknowledge financial support provided in the form of startup funds, the New Faculty Research Award, and the URSCO Undergraduate Research and Creativity Award (URCA) from the University of North Carolina at Greensboro. The Joint School of Nanoscience and Nanoengineering is acknowledged for providing access to the X-ray diffraction facility. We are also thankful to Dr. Maxime A. Siegler for helpful discussions on the X-ray crystallography.

References

1. M. Wikström, K. Krab, V. Sharma, Oxygen activation and energy conservation by cytochrome c oxidase, Chem. Rev. 118 (2018) 2469–2490.
2. B.F. Van Gelder, H. Beinert, Studies of the heme components of cytochrome c oxidase by EPR spectroscopy, Biochim. Biophys. Acta Bioenerg. 189 (1969) 1–24.
3. E.P. Day, J. Peterson, M.S. Sendova, J. Schoonover, G. Palmer, Magnetization of fast and slow oxidized cytochrome c oxidase, Biochemistry 32 (1993) 7855–7860.
4. Y.C. Fann, I. Ahmed, N.J. Blackburn, J.S. Boswell, M.L. Verkhovskaya, B. M. Hoffman, M. Wikström, Structure of CuB in the binuclear heme-copper center of the cytochrome aa3-type quinol oxidase from Bacillus subtilis: An ENDOR and EXAFS study, Biochemistry 34 (1995) 10245–10255.
5. S. Han, Y.-c. Ching, D.L. Rousseau, Ferryl and hydroxy intermediates in the reaction of oxygen with reduced cytochrome c oxidase, Nature 348 (1990) 89–90.
6. V. Sharma, K.D. Karlin, M. Wikström, Computational study of the activated OH state in the catalytic mechanism of cytochrome c oxidase, Proc. Natl. Acad. Sci. U. S. A. 110 (2013) 16844.
7. W.-G. Han Du, D. McRee, A.W. Götz, L. Noodleman, A water molecule residing in the $Fea_3^{3+}\cdots CuB^{2+}$ dinuclear center of the resting oxidized as-isolated cytochrome c oxidase: a density functional study, Inorg. Chem. 59 (2020) 8906–8915.
8. L. Noodleman, W.-G. Han Du, D. McRee, Y. Chen, T. Goh, A.W. Götz, Coupled transport of electrons and protons in a bacterial cytochrome c oxidase—DFT calculated properties compared to structures and spectroscopies, Phys. Chem. Chem. Phys. 22 (2020) 26652–26668.

9. R. Andersson, C. Safari, R. Dods, E. Nango, R. Tanaka, A. Yamashita, T. Nakane, K. Tono, Y. Joti, P. Båth, E. Dunevall, R. Bosman, O. Nureki, S. Iwata, R. Neutze, G. Brändén, Serial femtosecond crystallography structure of cytochrome c oxidase at room temperature, Sci. Rep. 7 (2017) 4518.

10. A. Nanthakumar, S. Fox, N.N. Murthy, K.D. Karlin, N. Ravi, B.H. Huynh, R. D. Orosz, E.P. Day, K.S. Hagen, N.J. Blackburn, Oxo- and hydroxo-bridged (porphyrin)iron(III)-copper(II) species as cytochrome c oxidase models: acid-base interconversions and X-ray structure of the Fe(III)-(O^{2-})-Cu(II) complex, J. Am. Chem. Soc. 115 (1993) 8513–8514.

11. K.D. Karlin, A. Nanthakumar, S. Fox, N.N. Murthy, N. Ravi, B.H. Huynh, R. D. Orosz, E.P. Day, X-ray structure and physical properties of the oxo-bridged complex [(F_8-TPP)Fe-O-Cu(TMPA)]$^+$, F_8-TPP = Tetrakis(2,6-difluorophenyl) porphyrinate(2-), TMPA = Tris(2-pyridylmethyl)amine: Modeling the cytochrome c oxidase Fe-Cu heterodinuclear active site, J. Am. Chem. Soc. 116 (1994) 4753–4763.

12. S. Hematian, I. Garcia-Bosch, K.D. Karlin, Synthetic heme/copper assemblies: Toward an understanding of cytochrome c oxidase interactions with dioxygen and nitrogen oxides, Acc. Chem. Res. 48 (2015) 2462–2474.

13. Titration experiments for determining the pK_a values for such complexes have been limited given the lack of availability of a comprehensive library of acids with continuous pK_a range that are soluble in organic solvents, along with their interferences due to undesirable coordinating ability of counteranions or solvents used.

14. S. Fox, A. Nanthakumar, M. Wikström, K.D. Karlin, N.J. Blackburn, XAS structural comparisons of reversibly interconvertible oxo- and hydroxo-bridged heme-copper oxidase model compounds, J. Am. Chem. Soc. 118 (1996) 24–34.

15. M.C. Carrasco, S. Hematian, (Hydr)oxo-bridged heme complexes: From structure to reactivity, J. Porphyrins Phthalocyanines 23 (2019) 1286–1307.

16. M.-A. Kopf, Y.-M. Neuhold, A.D. Zuberbuhler, K.D. Karlin, Oxo- and hydroxo-bridged heme-copper assemblies formed from acid–base or metal–dioxygen chemistry, Inorg. Chem. 38 (1999) 3093–3102.

17. H.V. Obias, G.P.F. van Strijdonck, D.-H. Lee, M. Ralle, N.J. Blackburn, K.D. Karlin, Heterobinucleating ligand-induced structural and chemical variations in [(L)Fe^{III}–O–Cu^{II}]$^+$ μ-oxo complexes, J. Am. Chem. Soc. 120 (1998) 9696–9697.

18. The pK_a values are reported in MeCN as it is the organic solvent with the most comprehensive pK_a scale. Also, the titrations were performed for 1 in both MeCN and DCM and the pK_a values for 1-Hþ were similar (i.e., 13.1 and 13.3, respectively). Here, DCM was chosen as the optimal solvent for our study due to its moderate polarity and non-coordinating nature.

19. C. Hansch, A. Leo, R.W. Taft, A survey of hammett substituent constants and resonance and field parameters, Chem. Rev. 91 (1991) 165–195.

20. A. Nanthakumar, S. Fox, N.N. Murthy, K.D. Karlin, Inferences from the ^{1}H-NMR spectroscopic study of an antiferromagnetically coupled heterobinuclear Fe(III)–(X)–Cu(II) S = 2 Spin System (X = O^{2-}, OH^{-}), J. Am. Chem. Soc. 119 (1997) 3898–3906.

21. J.M. Carroll, J.R. Norton, Protonation of a bridging oxo ligand is slow, J. Am. Chem. Soc. 114 (1992) 8744–8745.

22. It is important to note that in previous reports, upon protonation of the μ-oxoheme/Cu complex the upfield signals of the TMPA moiety disappeared at room temperature which was ascribed to the relatively weak M–OH bonds and partial dissociation of the complexes [16, 20]. We believe that this was mainly due to the use of coordinating solvent and counteranions.

23. I.M. Kolthoff, M.K. Chantooni, Protonation in acetonitrile of water, alcohols, and diethyl ether, J. Am. Chem. Soc. 90 (1968) 3320–3326.

24. ^{1}H-NMR spectrum of an authentic sample of $[(F_8TPP)Fe^{III}(THF)_2]^{+}$ and $[(tmpa)Cu^{II}(MeCN)]^{2+}$ were also recorded for comparison with the final reaction mixture and confirmed the dissociation process. Also, UV-vis profiles of the final reaction mixtures of all three systems discussed here are identical to those of the corresponding $[(P)Fe^{III}(THF)_2]^{+}$ authentic samples.

25. J. Wang, M.P. Schopfer, S.C. Puiu, A.A.N. Sarjeant, K.D. Karlin, Reductive coupling of nitrogen monoxide (•NO) facilitated by heme/copper complexes, Inorg. Chem. 49 (2010) 1404–1419.

26. E.J. Moore, J.M. Sullivan, J.R. Norton, Kinetic and thermodynamic acidity of hydrido transition-metal complexes. 3. Thermodynamic acidity of common mononuclear carbonyl hydrides, J. Am. Chem. Soc. 108 (1986) 2257–2263.

27. S.S. Kristjánsdóttir, J.R. Norton, A. Dedieu (Ed.), Transition Metal Hydrides: Recent Advances in Theory and Experiment, VCH, New York, 1992.

28. H. Kitagishi, D. Shimoji, T. Ohta, R. Kamiya, Y. Kudo, A. Onoda, T. Hayashi, J. Weiss, J.A. Wytko, K. Kano, A water-soluble supramolecular complex that mimics the heme/copper hetero-binuclear site of cytochrome c oxidase, Chem. Sci. 9 (2018) 1989–1995.

29. K.M. McCauley, J.M. Vrtis, J. Dupont, W.A. van der Donk, Insights into the functional role of the tyrosine–histidine linkage in cytochrome c oxidase, J. Am. Chem. Soc. 122 (2000) 2403–2404.

30. M. Aki, T. Ogura, Y. Naruta, T.H. Le, T. Sato, T. Kitagawa, UV resonance Raman characterization of model compounds of Tyr244 of bovine cytochrome c oxidase in its neutral, deprotonated anionic, and deprotonated neutral radical forms: Effects of covalent binding between tyrosine and histidine, J. Phys. Chem. A 106 (2002) 3436–3444.

31. J.A. Cappuccio, I. Ayala, G.I. Elliott, I. Szundi, J. Lewis, J.P. Konopelski, B.A. Barry, Ó. Einarsdóttir, Modeling the active site of cytochrome oxidase: Synthesis and characterization of a cross-linked histidine–phenol, J. Am. Chem. Soc. 124 (2002) 1750–1760.

32. A. Offenbacher, K.N. White, I. Sen, A.G. Oliver, J.P. Konopelski, B.A. Barry, Ó. Einarsdóttir, A spectroscopic investigation of a tridentate Cu-complex mimicking the

tyrosine–histidine cross-link of cytochrome c oxidase, J. Phys. Chem. B 113 (2009) 7407–7417.

33. V. Sharma, M. Wikström, The role of the K-channel and the active-site tyrosine in the catalytic mechanism of cytochrome c oxidase, Biochim. Biophys. Acta Bioenerg. 1857 (2016) 1111–1115.